RSC Advances

PAPER

View Article Online
View Journal | View Issue

Cite this: *RSC Adv.*, 2017, **7**, 35105

Effect of Y doping on high-pressure behavior of Ag_2S nanocrystals†

Pan Wang,[ab] Rui Zhao,[c] Lixin Wu[b] and Mingzhe Zhang *[a]

The effect of the dopant Y on high-pressure-induced polymorph transformation was investigated in Ag_2S nanocrystals. A polymorph transformation from monoclinic $P2_1/n$ phase I (where Ag1 and Ag2 atoms both participated in four-fold-coordinated tetrahedra) to orthorhombic $P2_12_12_1$ phase II (where Ag2 participated in four-fold-coordinated distorted tetrahedra but Ag1 in five-fold-coordinated pyramids) and then to another monoclinic $P2_1/n$ phase III (where Ag1 was still in the five-coordination pyramid-like structure but Ag2 showed a coordination number of five to form trigonal bipyramids) was observed under increasing high pressure at room temperature. The initial monoclinic phase was fully recovered after decompression. Compared with the two transition pressure values of the pure Ag_2S sample, those of the Y-doped sample were found to be lower, revealing the significant influence of even a low Y dopant concentration on the compressibility of Ag_2S. The smaller bulk modulus and larger volume collapse of the Ag_2S:Y sample further suggested it to be more compressible.

Received 11th May 2017
Accepted 3rd July 2017

DOI: 10.1039/c7ra05327d

rsc.li/rsc-advances

Introduction

As an important member of the family of semiconducting metal sulfides, silver sulfide (Ag_2S) nanocrystals have attracted great interest. They have a narrow band gap (1.0 eV), thereby emitting light of near-infrared (NIR) wavelengths.[1–6] Silver sulfide (Ag_2S) nanocrystals show potential in thermoelectric and optoelectronic materials, such as photovoltaic cells, gas sensors, sensitized solar cells, superionic conductors and infrared radiation detectors.[7–11] The applications of silver sulfide in realizing atomic switches, resistance switches and core–shell coaxial nanostructures have made this material especially attractive and a promising candidate for nanoscale electronics.[12,13] The ability to tune the electronic structures of semiconductors away from their pristine states is fundamental to semiconductor research, because this capability could lead to novel electronic and opto-electronic functionalities.[14] External pressure is well known as a powerful method to continuously tune atomic arrangements and the resulting properties away from those of the pristine states, and such tuning is crucial to a wide array of applications.[15–23] Doping could change the kind of carrier used and introduce an impurity band in the semiconductor, and such an impurity band can alter the electronic structure and corresponding optoelectronic properties.[24–26] The radius and electronegativity of a dopant differ from those of the cations in the host material, and a nonhomogeneous distribution of dopants, *i.e.*, the formation of areas enriched with doped ions but also some isolated doped ions, can cause lattice distortions and reduce the stability of the structure, leading to a significant influence on the phase transition.[27] Yttrium is an important member of the rare earth family and has been extensively utilized for making iron-, nickel-, and cobalt-based alloys, but has been little used as a dopant for modifying the properties and catalytic applications of a host material.[28]

It is of fundamental importance to understand how the crystal structural of Ag_2S changes under controlled external conditions. The polymorph transformation of silver sulfide resulting from changing the temperature has been studied extensively. At room temperature and ambient pressure, Ag_2S has a monoclinic crystal structure called α-Ag_2S, and known as the mineral acanthite at temperatures below ~450 K.[29] Upon increasing the temperature, a structural phase transition occurs at 453 K from the ordered monoclinic α-structure to the disordered body-centered cubic β-structure with the mineral named argentite.[30,31] The high-temperature face-centered cubic phase, γ-Ag_2S, is stable from a temperature of ~860 K until its melting point.[32,33] Less attention has been paid to the high-pressure-induced polymorph transformation in Ag_2S materials. Ag_2S experiences the phase transition sequence $P2_1/n \rightarrow P2_12_12_1 \rightarrow P2_1/n \rightarrow Pnma$ at hydrostatic pressures of ~5.1 GPa, 8.8 GPa, and 28.4 GPa, respectively.[14,34] Electrical transport measurements up to ~19 GPa combined with first-principles calculations showed that Ag_2S remained semiconducting while exhibiting dramatic changes in the concentration and mobility of the majority carrier.[35] However, to the best of our knowledge,

[a]State Key Laboratory of Superhard Materials, Jilin University, Changchun 130012, China. E-mail: zhangmz@jlu.edu.cn

[b]State Key Laboratory of Supramolecular Structure and Materials, Jilin University, Changchun 130012, China

[c]College of Computer, Jilin Normal University, Siping 136000, China

† Electronic supplementary information (ESI) available: Additional XPS analysis and the evolution of normalized cell parameters. See DOI: 10.1039/c7ra05327d

there has been no report on the effect of dopants on the high-pressure behavior of Ag_2S nanocrystals.

In this work, using *in situ* high-pressure synchrotron X-ray diffraction, we compared the compressibility of the pure and Y-doped Ag_2S nanocrystals. The two samples both experienced pressure-induced transitions from monoclinic $P2_1/n$ phase I to orthorhombic $P2_12_12_1$ phase II and then to another monoclinic $P2_1/n$ phase III. The initial monoclinic phase was fully recovered after decompression. Compared with the two transition pressure values of the pure Ag_2S sample, those of the Y-doped sample were found to be lower, revealing the significant influence of even a low Y dopant concentration on the compressibility of Ag_2S. The smaller bulk modulus and larger volume collapse of the Ag_2S:Y sample further suggested it to be more compressible.

Experimental methods

Pure and Y-doped Ag_2S nanocrystals were synthesized by carrying out a gas–liquid phase chemical deposition.[36] In the first step of the synthesis of Ag_2S:Y nanocrystals, $AgCOOCH_3$, $Y(NO_3)_3$, PVP, and deionized water were mixed to form a reaction solution. The molar ratio of Y^{3+} to Ag^+ was 0.18 in the reaction solution. In the first step of the synthesis of undoped Ag_2S nanocrystals, $AgCOOCH_3$, PVP, and deionized water were mixed to form the reaction solution. The dosage of PVP was 0.1 mg per litre in the reaction solution. In the reaction process, excess H_2S gas was introduced into a chamber with circulating water (25 °C) and reacted with the reaction solution. The above chamber was placed in an ultrasonic bath to avoid the agglomeration of reaction products and to generate convective motions in the liquid, which could make reaction solution in the bottom react with H_2S gas sufficiently and homogeneously. Finally, the reaction products were washed thrice by centrifugation with deionized water and anhydrous alcohol respectively, and dried in a nitrogen atmosphere. The phase impurity, structure, and crystal size of the above synthesized samples were characterized by analyzing X-ray diffraction (XRD) data recorded on an X-ray power diffractometer (Shimadzu, XRD-6000) with Cu Kalpha radiation (λ = 1.5406 Å), and high-resolution transmission electron microscopy (HRTEM) images acquired using a JEOL JEM-2200FS at 200 kV at ambient conditions. X-ray photoelectron spectroscopy (XPS) (ESCALAB MK II) was used to determine whether impurity elements were present and to determine the valence states of these elements.

In situ high-pressure synchrotron angle-dispersive XRD (ADXRD) experiments were conducted at the Cornell High Energy Synchrotron Source (λ = 0.485946 Å) at room temperature. High pressure was generated by using a symmetric diamond anvil cell (DAC) with 400 μm-diameter culets. Silicone oil was used as the pressure-transmitting medium. The samples and medium were loaded into a 150 μm-diameter hole drilled in the center of the pre-indented T301 stainless steel gasket. The pressure was calibrated by the frequency shift of the ruby R1 fluorescence line. The Bragg diffraction rings were recorded by using a MAR345 CCD detector. The two-dimensional diffraction patterns were integrated into one-dimensional profiles of intensity *versus* 2-theta with the program FIT2D, followed by the Materials Studio and POWDERCELL structural Rietveld refinement.

Results and discussion

The lower and upper panels of Fig. 1a show XRD patterns of, respectively, the pure and Y-doped Ag_2S nanocrystals at ambient conditions. The peak positions of all samples were consistent with those of the pure monoclinic structure of Ag_2S (JCPDS, No. 14-72). The XRD peaks of the Ag_2S:Y sample were found to be slightly shifted to higher angles relative to those of the pure Ag_2S sample, with this shift suggesting a decreased d spacing due to the Y dopant. The Rietveld full-profile refinement of the XRD patterns of the above two samples at ambient pressure yielded $a = 4.220 \pm 0.001$ Å, $b = 6.916 \pm 0.002$ Å, $c = 7.853 \pm 0.003$ Å, and $\beta = 99.651° \pm 0.023°$ for the pure Ag_2S nanocrystals, and $a = 4.213 \pm 0.001$ Å, $b = 6.904 \pm 0.001$ Å, $c = 7.839 \pm 0.001$ Å, $\beta = 99.639° \pm 0.014°$ for the Y-doped Ag_2S nanocrystals. The smaller lattice determined for the Ag_2S:Y sample suggested the existence of a lattice compression phenomenon as a result of having substituted Ag^+ (radius of 1.15 Å) with the smaller Y^{3+} ion (radius of 0.90 Å). No impurity phases corresponding to yttrium sulfides, yttrium oxides or silver oxides were detected above the XRD detection limit in either sample, indicating that Y^{3+} ions may have substituted for Ag^+ ions without changing the monoclinic structure of Ag_2S. The particle sizes of the two samples were estimated using Scherrer's formula to be about 30–32 nm.

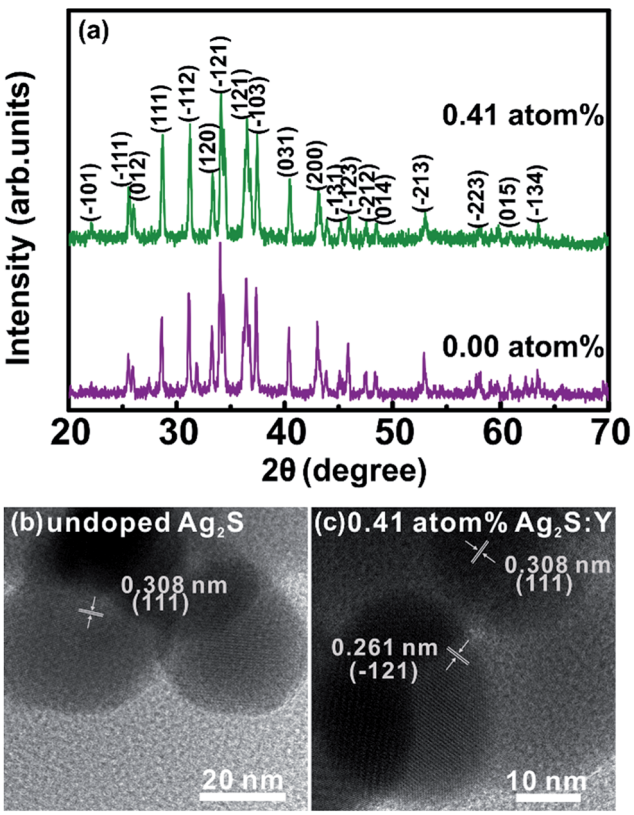

Fig. 1 (a) XRD patterns and (b and c) HRTEM images of pure and 0.41 atom% Ag_2S nanocrystals at ambient conditions.

The microstructures of the pure and Y-doped Ag_2S nanocrystals were further investigated using HRTEM. As shown in Fig. 1b, the interplanar spacing of the undoped Ag_2S nanocrystals was measured to be 0.308 nm, consistent with (111) lattice plane of the monoclinic Ag_2S structure. Individual particles were clearly observed in the pure Ag_2S sample image (Fig. 1b), and measured to have diameters between about 30 and 32 nm. Interplanar spacings of 0.308 nm and 0.261 nm were measured for the Ag_2S:Y nanocrystals (Fig. 1c), consistent with the (111) and (−121) lattice planes of the monoclinic Ag_2S structure, respectively. The particle size of the Ag_2S:Y samples was observed to also be about 30–32 nm. According to our XPS analysis (ESI, Fig. S1 and Table S1†), Y was in the Y^{3+} state in the host Ag_2S semiconductor, and the Y content was about 0.41 atom% in the Y-doped Ag_2S nanocrystals.

Fig. 2 shows the ADXRD data of the pure Ag_2S and 0.41 atom% Ag_2S:Y nanocrystals at several selected pressure levels at room temperature. As shown in Fig. 2a, for the pure Ag_2S nanocrystals, all diffraction peaks shifted toward higher angles (larger d spacings) and broadened noticeably with increasing pressure. At the lowest measured pressure of 0.93 GPa, the pure Ag_2S nanocrystals formed the monoclinic $P2_1/n$ phase (phase I), which was consistent with the ambient condition structure. When the pressure was increased, a structural transition first occurred at 6.83 GPa, with new peaks (marked by asterisks) belonging to the orthorhombic Ag_2S phase (space group $P2_12_12_1$) (phase II), isostructural to the ambient condition structure (mineral naumannite) of Ag_2Se. Note that pure phase II was not detected in the phase transformation because of the similar energy levels of phase I and phase II.[14,34] This phase II was stable up to 9.30 GPa, where another transition took place. At this point, a $P2_1/n$ phase III structure isosymmetric to the phase I structure started to appear (marked by asterisks) and the peaks corresponding to the phase II gradually lost intensity. Both phases coexisted between this pressure and 11.80 GPa. All of the peaks of the phase II completely disappeared when the pressure was increased to 11.80 GPa, indicating completion of the phase transition. Phase III was stable up to the highest pressure of 19.30 GPa in this experiment.

A similar phase transition process was indicated by the results of synchrotron ADXRD experiments (Fig. 2b) of 0.41 atom% Ag_2S:Y nanocrystals at room temperature up to 18.61 GPa. As displayed in Fig. 2b, with the increasing pressure, two pressure-induced structural transitions of the Ag_2S:Y sample occurred, at 5.90 and 9.00 GPa, which were lower than those of the pure Ag_2S nanoparticles.

For the pure Ag_2S sample (Fig. 3a), as the pressure was decreased to 16.50 GPa, the phase II diffraction peaks started to appear. Further lowering the pressure to 2.8 GPa resulted in a transformation of the diffraction peaks to those of phase I. When the pressure was lowered to the ambient pressure (Fig. 3), the shapes of all of the diffraction peaks of both samples returned to those of the initial monoclinic phase I structure, indicating the reversibility of the pressure-induced structural transformation. The refinement results of the lattices of the recovered samples were to be $a = 4.217 \pm 0.001$ Å, $b = 6.895 \pm 0.002$ Å, $c = 7.840 \pm 0.001$ Å, and $\beta = 99.703° \pm 0.015$ for the pure Ag_2S sample, and $a = 4.217 \pm 0.003$ Å, $b = 6.895 \pm 0.001$ Å, $c = 7.838 \pm 0.001$ Å, and $\beta = 99.622° \pm 0.018$ for the Ag_2S:Y sample, both slightly smaller than those of the samples prior to compression.

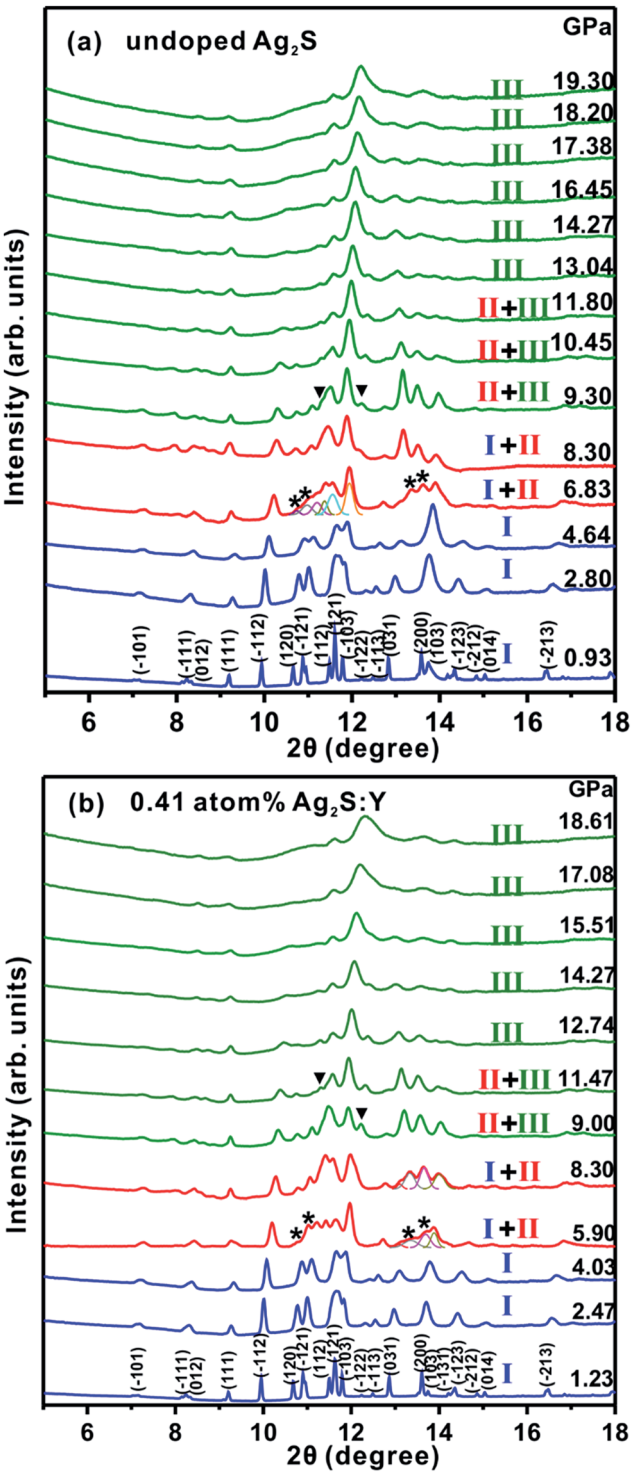

Fig. 2 Synchrotron-derived angle-dispersive XRD patterns of (a) pure Ag_2S and (b) 0.41 atom% Ag_2S:Y nanocrystals were recorded for pressure increase at room temperature. The radiation wavelength was 0.485946 Å. Asterisks and inverted triangles indicate diffraction peaks found only for phase II or phase III, respectively.

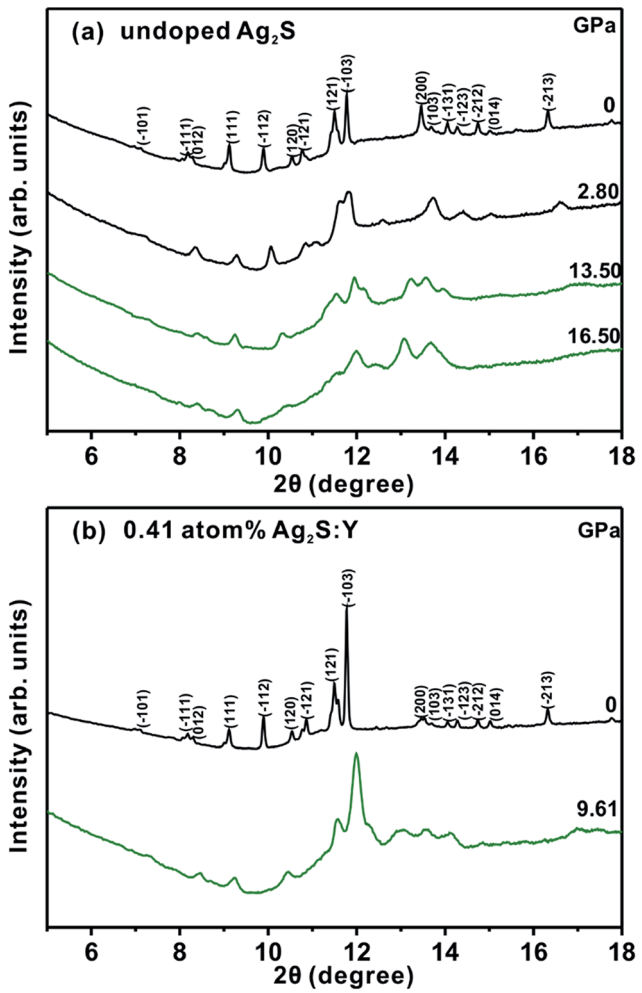

Fig. 3 Synchrotron-derived angle-dispersive XRD patterns of (a) pure Ag_2S and (b) 0.41 atom% Ag_2S:Y nanocrystals were recorded for pressure decrease at room temperature. The radiation wavelength was 0.485946 Å. Asterisks indicate diffraction peaks found only for phase II.

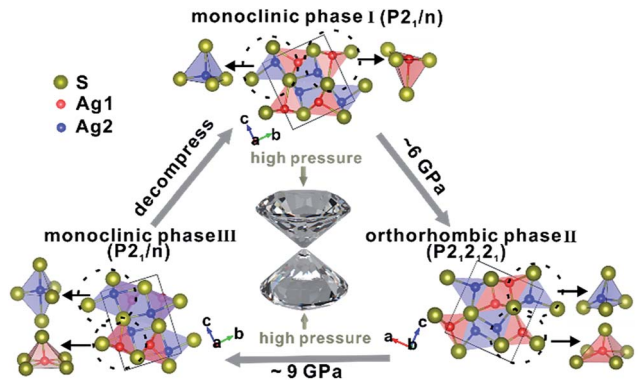

Fig. 4 Schematic structures of the phase I, II, and III unit cells of the Ag_2S compounds. The pressures of the phase transitions during compression and decompression sequences are also indicated.

The evolution of the normalized cell parameters (ESI, Fig. S3†) and crystal structures (Fig. 4) for the three phases were investigated to reveal the phase transformation route. As displayed in Fig. 4, phase I showed a distorted anti-$PbCl_2$-type structure, where Ag1 and Ag2 atoms both showed four-fold coordination. During the initial compression, the contraction of the lattice parameters was rather anisotropic and the *b* axis was found to be the most compressible of the lattice constants, as indicated in the obtained evolution of the normalized cell parameters of the phase I (ESI file, Fig. S3a†). In phase II, two Ag sites were still observed within the structure. Ag2 was four-fold coordinated to form distorted tetrahedra. In contrast, Ag1 increased from being four-fold to five-fold coordinated to form pyramids.[14] The phase II structure was observed to be less compressible along its *a* and *b* axes than the *c* axis, as shown in Fig. S3b (ESI†). In the phase III structure, the coordination number of Ag1 was maintained at five (and showed a pyramid-like structure), but that of Ag2 increased from four to five to form a trigonal bipyramid.[14] The *b* axis of the phase III structure was observed to be the most compressible of its lattice constants, and its *c* axis was indicated to be almost incompressible (Fig. S3c, ESI†).

We combined the Rietveld refinement results in order to fit *P–V* data of the pure Ag_2S and 0.41 atom% Ag_2S:Y nanocrystals to the Birch–Murnaghan (BM) equation of state (EOS), which could shed light on the effect of dopant Y on the polymorph

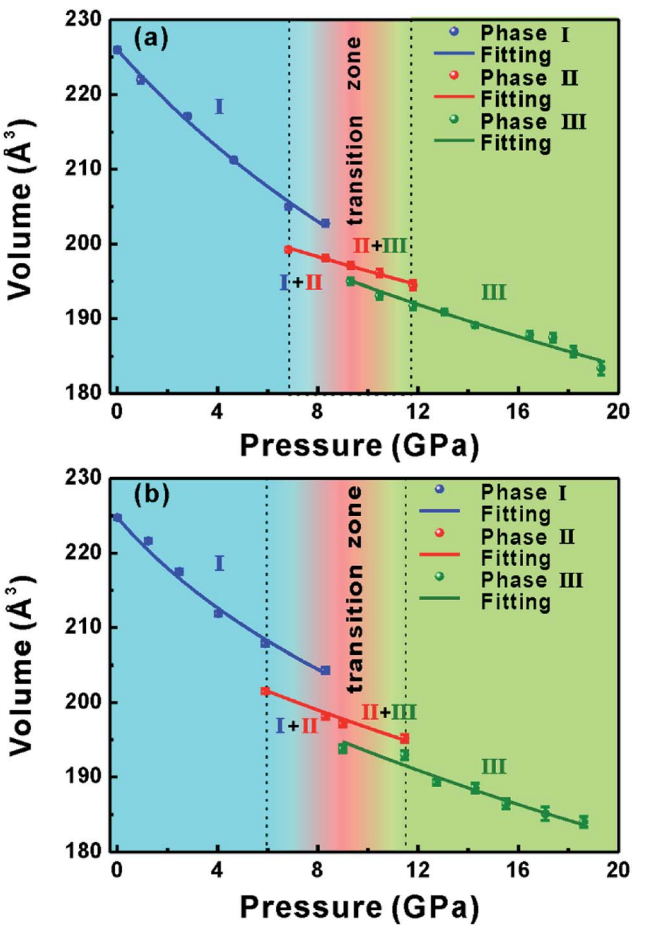

Fig. 5 Pressure–volume diagrams of (a) pure Ag_2S and (b) 0.41 atom% Ag_2S:Y nanocrystals.

transformation of Ag_2S, as shown in Fig. 5, where only the compressional data were used for EOS fitting. A third-order BM equation of state was fitted to the plot of the unit cell volume of the phase I structure *versus* pressure, and the zero-pressure volume (V_0) was considered to be the experimentally determined unit cell volume value. We obtained a bulk modulus B_0 of 59.7(4) GPa (V_0 = 225.9 Å^3) and first pressure derivative B' of 4.2(3) for the pure Ag_2S, and B_0 of 57.3(6) GPa (V_0 = 224.8 Å^3) and B' of 8.5(4) for the Ag_2S:Y nanocrystals. For the phase II and phase III data, a second-order Birch–Murnaghan was employed. B_0 and V_0 were left to vary freely, and the B' was fixed to 4. For the phase II structure, the EOS parameters were determined to be $V_0 = 210.1(2)$ Å^3 and $B_0 = 168.5(3)$ GPa for the pure Ag_2S, and V_0 = 207.1(7) Å^3 and B_0 = 131.6(8) GPa for the Ag_2S:Y nanocrystals. For phase III, we obtained V_0 = 208.9(4) Å^3 and B_0 = 123.1(0) GPa for the pure Ag_2S, and V_0 = 208.5(6) Å^3 and B_0 = 111.2(5) GPa for Ag_2S:Y nanocrystals.

The percentage decreases of the unit cell volumes from phase I to phase II at 6.83 GPa and 5.9 GPa were 2.825% and 3.063% for the pure Ag_2S and Ag_2S:Y nanocrystals, and those from phase II to phase III at 9.30 GPa and 9.00 GPa were 1.092% and 1.698% for the pure Ag_2S and Ag_2S:Y nanocrystals, respectively. The smaller bulk modulus B_0 and larger decrease in volume for the Ag_2S:Y sample than for the pure Ag_2S sample further suggested a larger compressibility for the Ag_2S:Y sample, which indicated that even a low concentration of the Y dopant had a significant influence in the compressibility. The dopant can induce vacancy and substitution defects in crystal lattices resulting in lattice distortion, thus eventually reducing the stability of lattice structure.[27,37]

Conclusions

In summary, the effect of dopant Y on high-pressure-induced polymorph transformation was investigated in Ag_2S nanocrystals. A polymorph transformation from monoclinic $P2_1/n$ phase I (where Ag1 and Ag2 atoms both participated in four-fold-coordinated tetrahedra) to orthorhombic $P2_12_12_1$ phase II (where Ag2 participated in four-fold-coordinated distorted tetrahedra but Ag1 in five-fold-coordinated pyramids) and then to another monoclinic $P2_1/n$ phase III (where Ag1 was still in the five-coordination pyramid-like structure but Ag2 showed a coordination number of five to form trigonal bipyramids) was observed under increasing high pressure at room temperature. The initial monoclinic phase was fully recovered after decompression. Compared with the two transition pressure values of the pure Ag_2S sample, those of the Y-doped sample were found to be lower, revealing the significant influence of even a low Y dopant concentration on the compressibility of Ag_2S. The smaller bulk modulus and larger volume collapse of the Ag_2S:Y sample further suggested it to be more compressible.

Acknowledgements

This work was funded by the National Science Foundation of China, No. 11174103 and 11474124.

Notes and references

1 K. Hickman and W. Weyerts, *Nature*, 1933, **132**, 134–135.
2 H. Doh, S. Hwang and S. Kim, *Chem. Mater.*, 2016, **28**, 8123–8127.
3 Y. P. Du, B. Xu, T. Fu, M. Cai, F. Li, Y. Zhang and Q. B. Wang, *J. Am. Chem. Soc.*, 2010, **132**, 1470–1471.
4 G. S. Hong, J. T. Robinson, Y. J. Zhang, S. Diao, A. L. Antaris, Q. B. Wang and H. J. Dai, *Angew. Chem., Int. Ed.*, 2012, **124**, 9956–9959.
5 F. D. Duman, I. Hocaoglu, D. G. Ozturk, D. Gozuacik, A. Kiraz and H. Y. Acar, *Nanoscale*, 2015, **7**, 11352–11362.
6 W. Jiang, Z. Wu, X. Yue, S. Yuan, H. Lu and B. Liang, *RSC Adv.*, 2015, **5**, 24064–24071.
7 C. Yu, M. Leng, M. Z. Liu, Y. Yu, D. Liu and C. Wang, *CrystEngComm*, 2012, **14**, 3772–3777.
8 P. Jiang, Z. Q. Tian, C. N. Zhu, Z. L. Zhang and D. W. Pang, *Chem. Mater.*, 2012, **24**, 3–5.
9 K. Terabe, T. Hasegawa, T. Nakayama and M. Aono, *Nature*, 2005, **433**, 47–50.
10 Y. Zhang, G. Hong, Y. Zhang, G. Chen, F. Li, H. Dai and Q. Wang, *ACS Nano*, 2012, **6**, 3695–3702.
11 J. Yang and J. Y. Ying, *Angew. Chem., Int. Ed.*, 2011, **50**, 4637–4643.
12 P. Chattopadhyay and S. G. Roy, *J. Appl. Phys.*, 2014, **116**, 133516.
13 T. Ohno, T. Hasegawa, A. Nayak, T. Tsuruoka, J. K. Gimzewski and M. Aono, *Appl. Phys. Lett.*, 2011, **99**, 203108.
14 Z. Zhao, H. Wei and W. L. Mao, *Appl. Phys. Lett.*, 2016, **108**, 261902.
15 G. J. Xiao, X. Y. Yang, X. X. Zhang, K. Wang, X. L. Huang, Z. H. Ding, Y. M. Ma, G. T. Zou and B. Zou, *J. Am. Chem. Soc.*, 2015, **137**, 10297–10303.
16 X. Yang, Q. Li, R. Liu, B. Liu, S. Jiang, K. Yang, J. Liu, Z. Chen, B. Zou, T. Cui and B. Liu, *CrystEngComm*, 2014, **16**, 4441–4446.
17 Z. H. Yu, L. Wang, Q. Y. Hu, J. G. Zhao, S. Yan, K. Yang, S. Sinogeikin, G. Gu and H. K. Mao, *Sci. Rep.*, 2015, **5**, 15939.
18 Z. Zhao, H. J. Zhang, H. T. Yuan, S. B. Wang, Y. Lin, Q. S. Zeng, G. Xu, Z. X. Liu, G. K. Solanki, K. D. Patel, Y. Cui, H. Y. Hwang and W. L. Mao, *Nat. Commun.*, 2015, **6**, 7312.
19 M. C. Yang, R. C. Xiang, W. Qiang, Y. G. Hua, Z. Y. Xiao, X. W. Yi and W. W. Zi, *J. Phys. D: Appl. Phys.*, 2016, **49**, 355305.
20 G. Hong, L. Xin, Z. Zhenjie and X. Wenhui, *J. Phys. D: Appl. Phys.*, 2016, **49**, 055303.
21 J. P. Itié, E. Girard, N. Guignot, Y. L. Godec and M. Mezouar, *J. Phys. D: Appl. Phys.*, 2015, **48**, 504007.
22 H. Zhang, Q. Li, B. Cheng, Z. Guan, R. Liu, B. Liu, Z. Liu, X. Li, T. Cui and B. Liu, *RSC Adv.*, 2016, **6**, 104949–104954.
23 R. Zhao, P. Wang, B. Yao, T. Hu, T. Yang, B. Xiao, S. Wang, C. Xiao and M. Zhang, *RSC Adv.*, 2015, **5**, 17582–17587.
24 A. K. Guria and N. Pradhan, *Chem. Mater.*, 2016, **28**, 5224–5237.

25 X. Wang, B. Chang, L. Ren and P. Gao, *Appl. Phys. Lett.*, 2011, **98**, 082109.
26 L. Xu and X. Li, *J. Cryst. Growth*, 2010, **312**, 851–855.
27 B. B. Yao, H. Y. Zhu, S. M. Wang, P. Wang and M. Z. Zhang, *J. Solid State Chem.*, 2014, **210**, 150–154.
28 R. Sharma, Komal, V. Kumar, S. Bansal and S. Singhal, *Mater. Res. Bull.*, 2017, **90**, 94–103.
29 S. I. Sadovnikov, A. I. Gusev and A. A. Rempel, *Phys. Chem. Chem. Phys.*, 2015, **17**, 20495–20501.
30 O. Alekperov, Z. Jahangirli and R. Paucar, *Phys. Status Solidi B*, 2016, **253**, 2049–2055.
31 F. F. Aliev, M. B. Jafarov, B. A. Tairov, G. P. Pashaev, A. A. Saddinova and A. A. Kuliev, *Semiconductors*, 2008, **42**, 1146.
32 D. Živković, V. Ćosović, Ž. Živković, N. Štrbac, M. Sokić, N. Talijan, B. Boyanov and A. Mitovski, *Mater. Sci. Semicond. Process.*, 2013, **16**, 217–220.
33 S. I. Sadovnikov, A. V. Chukin, A. A. Rempel' and A. I. Gusev, *Phys. Solid State*, 2016, **58**, 30–36.
34 D. Santamaría-Pérez, M. Marqués, R. Chuliá-Jordán, J. M. Menendez, O. Gomis, J. Ruiz-Fuertes, J. A. Sans, D. Errandonea and J. M. Recio, *Inorg. Chem.*, 2012, **51**, 5289–5298.
35 J. K. Zhang, C. L. Liu, X. Zhang, F. Ke, Y. H. Han, G. Peng, Y. Z. Ma and C. X. Gao, *Appl. Phys. Lett.*, 2013, **103**, 082116.
36 P. Wang, T. Y. Yang, R. Zhao and M. Z. Zhang, *Phys. Chem. Chem. Phys.*, 2016, **18**, 10123–10128.
37 P. Wang, R. Zhao, Z. F. Li, T. Y. Yang and M. Z. Zhang, *CrystEngComm*, 2016, **18**, 2607–2611.